iScience

CellPress
OPEN ACCESS

Article

Parallel battery pack charging strategy under various ambient temperatures based on minimum lithium plating overpotential control

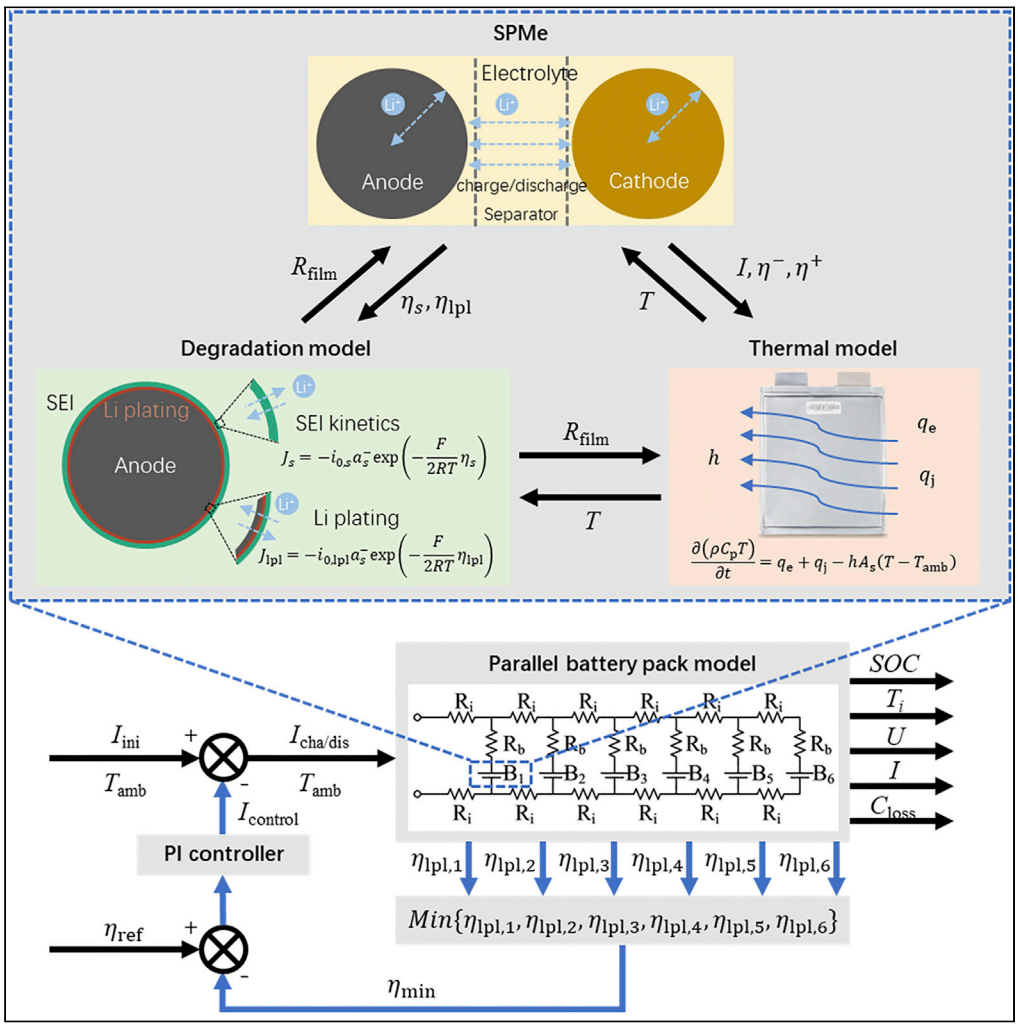

Hanqing Yu, Long Yang, Lisheng Zhang, Junfu Li, Xinhua Liu

lijunfu@hit.edu.cn (J.L.)
liuxinhua19@buaa.edu.cn (X.L.)

Highlights

A cell model is established accurately under various C-rates and temperatures

The contact and wire resistances are considered into the battery pack circuit model

Side reactions like Li plating are accurately described in the model during cycling

Charging strategy for parallel battery pack is adopted to prevent side reactions

Yu et al., iScience 25, 104243
May 20, 2022
https://doi.org/10.1016/j.isci.2022.104243

iScience

CellPress
OPEN ACCESS

Article

Parallel battery pack charging strategy under various ambient temperatures based on minimum lithium plating overpotential control

Hanqing Yu,[1,2] Long Yang,[1] Lisheng Zhang,[2] Junfu Li,[1,*] and Xinhua Liu[2,3,*]

SUMMARY

With the aggravation of environmental pollution and energy crisis, lithium-ion batteries are widely regarded as promising. However, the current distribution in the parallel battery pack branches is highly heterogeneous. Charging strategies based on the models can be adopted to prevent side reactions that may lead to severe degradation or even thermal runaway under various ambient temperatures. In this study, a battery model for a single cell is established by coupling a single particle model with electrolyte, degradation model, and thermal model. Besides, considering the contact resistance and wire resistance, the circuit model of a battery pack is established. A charging strategy based on minimum Li plating overpotential control is then adopted, and the effectiveness under high C-rate and low temperature to reduce capacity loss is verified by simulation. This study provides a low-loss charging strategy that can reduce the safety risk of battery packs with better performance under various ambient temperatures.

INTRODUCTION

As the aggravation of environmental pollution and energy crisis, the use of new energy has become a hotspot, such as new energy vehicles and energy storage systems. Lithium-ion batteries (LIBs) have been widely used because of stable discharge, low self-discharge rate, long cycle life, and other advantages (Chen et al., 2019; Zhao et al., 2021). However, a single cell is far from meeting the requirements of a system, so a large number of cells need to be connected in series or parallel with each other to form a battery pack. Compared to series battery packs, the current distribution of each branch for parallel battery pack is very inconsistent and complicated because of the resistances caused by the wire and welding (Hosseinzadeh et al., 2021; Wu et al., 2021). In addition, the current is closely related to the side reactions; performance of the battery packs will degenerate after some cycles (Tang et al., 2021). Meanwhile, with the continuous improvement of energy consumption level, there is an increasing demand for large-capacity new energy storage and power facilities, which requires corresponding digital life-cycle management solution (Yang et al., 2020; Wu et al., 2020; Gao et al., 2021), and charging technology is an important part.

LIB is a complicated system for its internal interaction. Thus, the mathematical relationship between environmental factors and battery characteristics should be determined by establishing the model, which is very important to optimize battery design and manage batteries (Zhou et al., 2022; Hosen et al., 2021). There are many battery models based on experience and data, such as the equivalent circuit model (ECM) and the data-driven model (Nikdel, 2014; Dang et al., 2016). However, they often do not fully reflect the overall state of the battery, so have certain limitations. There are many studies to establish models for predicting voltage based on the electrochemical properties of LIB. The most recognized model is the pseudo-two-dimensional (P2D) model proposed by Doyle et al. (1993). However, because the calculation process of the P2D model is too complicated and will consume too many computing resources, many studies have simplified it, among which the single particle model (SPM) is the most common one (Zhang et al., 2000). SPM ignores the concentration and potential changes in the electrolyte, which results in poor accuracy of the model, especially at large C-rates and low ambient temperatures. To solve this problem, a single particle model with electrolyte (SPMe) has been used (Li et al., 2021a). It improves the prediction accuracy by considering the influence of electrolyte. Besides, the electrochemical process of LIB also affects aging and heat generation. As for the aging process, side reactions on the anode have been the focus of research (Lu et al., 2021), and the processes of solid electrolyte interface (SEI) film growth and Li

[1]School of Automotive Engineering, Harbin Institute of Technology, Weihai, Shandong, China

[2]School of Transportation Science and Engineering, Beihang University, Beijing, China

[3]Lead contact

*Correspondence: lijunfu@hit.edu.cn (J.L.), liuxinhua19@buaa.edu.cn (X.L.)

https://doi.org/10.1016/j.isci.2022.104243

plating are usually modeled (Reniers et al., 2019). For the heat generation process, Bernardi et al. (1985) proposed a universal thermal model based on thermodynamic energy balance, which had been used in almost all studies of battery heat generation. However, the original model is complicated. Considering the characteristics of commercial batteries, some factors with relatively small effects can be ignored to simplify the model (Gottapu et al., 2021).

For parallel battery packs, the inconsistency of current distribution has been studied in many previous studies (Wu et al., 2013; Brand et al., 2016). In addition, ambient temperature is an important factor (Xie et al., 2021). Compared with single cells, different degradation behaviors at the battery pack level have also been reported (Shi et al., 2016; Wang et al., 2019). Dubarry et al. (2016) developed a useful equivalent circuit model to simulate the spontaneous transient balancing currents among parallel strings. The study could help understand transient behavior to help with battery management, maintenance, and repair. Schindler et al. (2020) further studied the influence of connection characteristics inside the battery pack on current distribution. It was found that cross-connectors could effectively balance the battery system. In addition, the study showed that string-connect resistances contributed more toward current distribution than welding seam and cross-connector resistances. In the previous study of Liu et al. (2019a), the circuit model of six parallel cells was established, and each single cell was realized by a thermally coupled single particle model. The effects of intercell variation and thermal gradient on the performance and degradation were studied in detail.

With the rapid increase of the demand for fast charging, battery charging technology has gradually attracted widespread interest. Tomaszewska et al. (2019) reviewed the literature on the physical phenomena that limit battery charging speeds, the degradation mechanisms that commonly result from charging at high currents, and the approaches that have been proposed to address these issues, which suggested that the problem of fast charging could be solved by developing battery multi-scale design and charging strategies. In terms of battery design, emerging materials that can improve battery performance are always the focus, such as electrodes with low tortuosity and electrolytes with high Li transference number, which can fundamentally improve the charging C-rate without serious degradation (Liu et al., 2019b; Peng et al., 2021; Yan et al., 2021). Based on already established commercial LIBs, there are also many fast charging strategies for health and efficiency, such as constant current-constant voltage (CC-CV), multistage constant-current (MCC), and pulse charging (Tomaszewska et al., 2019). These charging strategies are convenient but lack feedback from the battery itself. They may cause side reactions to affect battery performance and safety, and bring some additional risks, such as thermal runaway. Ouyang's group (Li et al., 2019) explained that the reaction between the plated lithium and electrolyte was revealed to be the mechanism of thermal runaway triggering and warned us of the danger of the plated lithium in the utilization of lithium-ion batteries. Thus, it is necessary to limit Li plating during fast charging. As a result, there are more and more studies on exploring charging strategies based on the characteristics of models (Zhang et al., 2017; Yang et al., 2021). In addition, it should be noted that because of the complex operating environment, the charging strategies must meet the requirements of fast charging under various ambient temperatures. There have also been some studies reported on fast charging at low ambient temperatures (Xie et al., 2020; Nambisan et al., 2021). However, most of these studies are based on ECM, which cannot reflect the physical information inside the battery. At the same time, most of them are based on existing charging protocols and lack precise feedback control.

However, it is difficult and important to study the fast charging strategy of battery packs because of the inconsistencies of cells. Ouyang et al. (2019) proposed a distributed charging strategy considering both charging time and capacity loss, which had low computational cost and high robustness. Li et al. (2021b) established a complete battery pack model by combining the cell model, battery pack cooling model, and battery pack balance management model. In addition, a fast charging strategy based on the shortest charging time was proposed. The results showed that the fast charging strategy could significantly shorten the charging time but would lead to increased aging and energy loss. In addition, there is no feedback in the established fast charge protocols, which cannot control the side reactions of batteries. However, the current of fast charging is relatively large. Besides, owing to the current inconsistency of parallel battery packs, the currents on some branches tend to reach a higher C-rate, which will lead to excessive degradation of the cell on the branch, resulting in accelerating degradation of the battery pack performance. These causes can easily cause serious harm to the electrochemical and safety performance of batteries leading to accelerated degradation (Tomaszewska et al., 2019; Wang et al., 2021a) or even catastrophic events like

thermal runaway under extreme conditions (Feng et al., 2020). At the same time, the fast charging and discharging is an important approach to improve the efficiency of vehicle-to-grid (V2G) storage configuration (Dioha et al., 2022). In this case, both vehicles and power grid energy storage facilities are faced with the problem of degradation in the process of fast charging. Therefore, it is necessary to design a model-based fast charging strategy, which can well control the occurrence of side reactions, and can significantly reduce the degradation of electrochemical and safety performance. Yang et al. (2019) reported a controllable cell structure, which could quickly heat the battery to high temperatures to eliminate lithium plating during charging. Chu et al. (2017) constructed a close-loop observer of lithium deposition status based on the simplified P2D model. The charging current was modified online using the feedback of the lithium deposition status. In addition, the postmortem observation and degradation tests were performed. The results showed that no lithium deposition occurred during fast charging.

In this paper, in terms of the fast charging strategy of parallel battery packs, an appropriate model should be established to control side reactions under various ambient temperatures, so as to prevent side reactions. Firstly, the cell model was established by coupling the SPMe, degradation model and thermal model. Then, considering the contact resistance and the wire resistance, the circuit model of the parallel battery pack was established. After that, based on the model, a parallel battery pack charging strategy based on minimum Li plating overpotential control (MLPOC) was adopted to realize the control of minimum Li plating. The closed-loop optimization framework of input current under various ambient temperatures was established. Finally, the simulation based on the model and charging control strategy was carried out, and the results were compared to verify the effectiveness of the proposed model and strategy.

RESULTS

Parallel battery pack model

In this chapter, a SPMe is developed for the single cell considering thermal effects and typical side reactions. In addition, six cells are parallel-connected to create a battery pack with current input and output on the one side. There is a branch resistance in each branch in series with the cell and an interconnect resistance at each end of each branch. There is also an electrochemical performance simulation of one particular cell in this chapter.

Single cell model

To better describe the behaviors of LIBs in fast charging and under various ambient temperatures, the single cell model can be divided into three main parts: SPMe, degradation model because of side reactions, and thermal model.

SPM is the most widely used simplified version of the P2D model, and is based on the following assumptions:

[A1] The concentration distribution within the electrolyte is ignored, and the potential of the liquid phase is assumed to be 0 V when calculating the terminal voltage.

[A2] The active material in each electrode region is abstracted as a single particle and the solid phase is homogeneous. This means that the potential of the anode and cathode in their respective regions is a fixed value and does not change with the change of position in the direction of the electrode plate thickness.

The thermally coupled SPM has been discussed in depth in our previous studies (Liu et al., 2019a; Yang et al., 2021). In this study, in order to improve the accuracy of the model and the applicability under various ambient temperatures, the Assumption [A1] is canceled and the SPMe is established by considering the concentration distribution and liquid phase potential within the electrolyte.

LIBs are mainly composed of anode, separator, and cathode and are filled with electrolyte inside. The basic structure of LIBs is shown in Figure 1. In the x direction, the compositions are superposed. Since the Assumption [A2], the active material in each electrode region can be approximately described as a spherical active material particle, respectively. The radial direction inside the particle is defined as r direction. For the convenience of describing the behavior of lithium-ions in electrolyte, the distribution of ion current

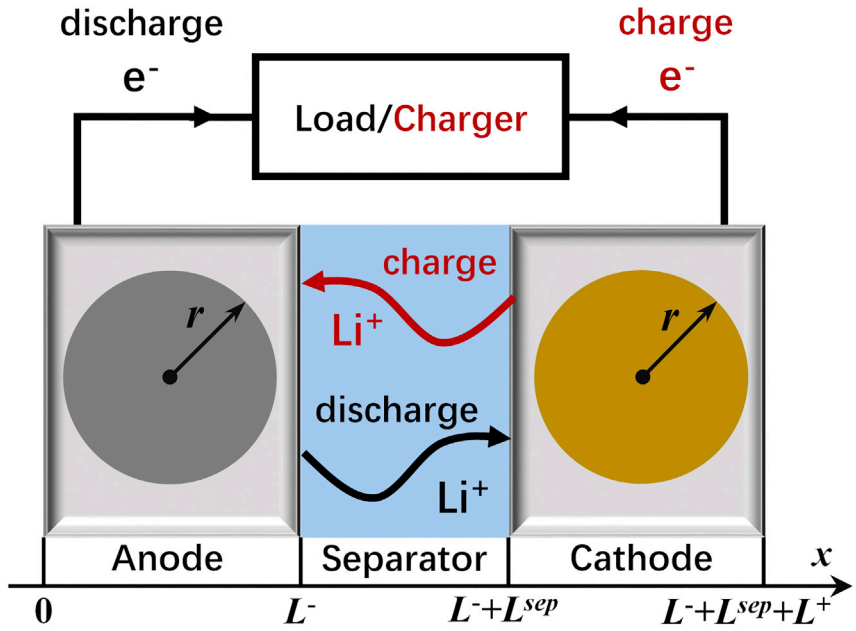

Figure 1. Schematic of the basic structure of LIBs

density i_e and molar ion flux j_n in the direction of the electrode plate thickness are shown in Figure 2. In addition, the block diagram of SPMe is shown in Figure 3.

Detailed descriptions for the three submodels of the single cell model are provided in Method details. They are related to each other. The coupling relationship among them is shown in Figure 4. At the top of the figure, there is the SPMe which works with lithium-ion transferred between the cathode and anode. It should be noted that lithium-ion must be intercalated or delaminated through the film on the anode surface. On the left of the figure, there is the degradation model which is used to calculate SEI film growth and Li plating. On the right of the figure, there is the thermal model, which considers both the heat generation and external natural convection heat dissipation. In the process of model calculation, the SPMe provided the current and reaction polarization overpotential for the thermal model to calculate the heat generation rate, and provided the side reaction overpotentials for the degradation model. The thermal model is used to determine the battery temperature and the influence of the electrochemical parameters in the SPMe and degradation models. The degradation model causes the increase of internal resistance and the capacity loss in SPMe, and the increase of internal resistance can lead to the increase of heat generation, thus affecting the thermal model.

In this work, the simulated cell was the pouch cell with capacity of 5 Ah, which contains NCM-LCO composite cathodes and graphite anodes. Specific parameters for the cell are shown in Table S1. The cell model is

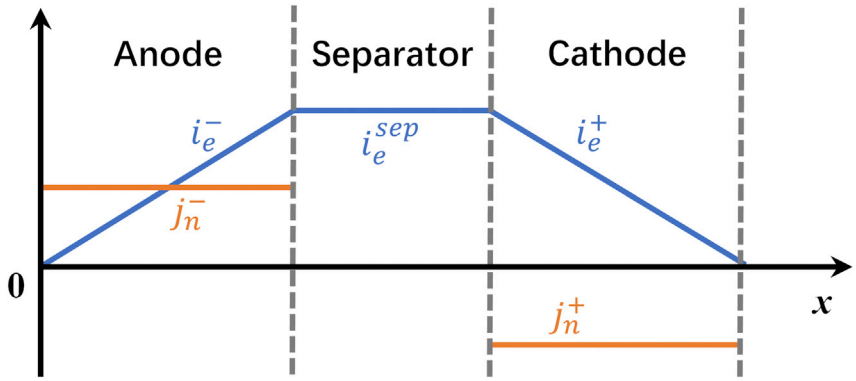

Figure 2. Simplified form of ionic current density i_e and molar ion fluxes j_n in the SPMe model

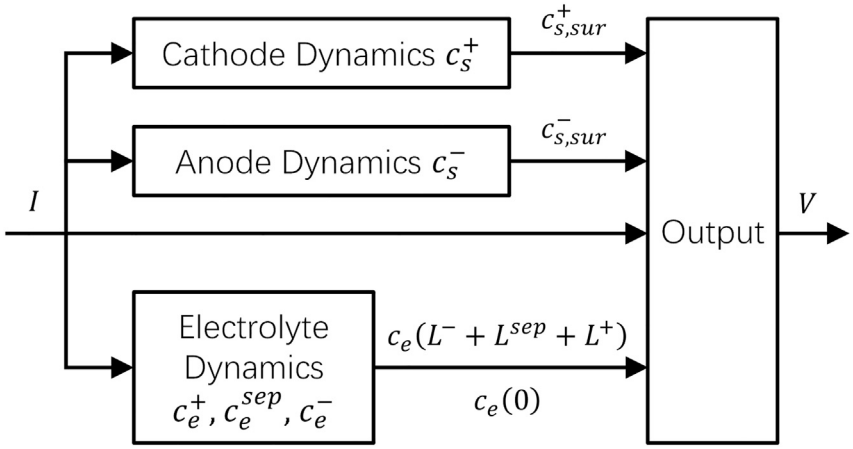

Figure 3. Block diagram of SPMe

further used in exploration of the charge strategy proposed later. Since the cell does not change much with the high ambient temperatures (Wang et al., 2021b), this study mainly investigates the performance of the cell with the low ambient temperatures because of the great influence on the side reactions. Figure 5 shows the simulation results of the single cell in the battery pack at different C-rates (0.5C, 1C, and 2C) and temperatures (−10°C, 0°C, 10°C, and 20°C). Figure 5A shows the change of cell voltage, and Figure 5B shows the change of cell temperature. For side reactions, the electrochemical overpotential of Li plating and the capacity loss caused by SEI growth and Li plating are shown in Figures 5C and 5D, respectively.

It should be noted from Figure 5A that with the increase of C-rate or the decrease of ambient temperature, the battery voltage curve with high C-rate, or low ambient temperature will be higher because of more serious polarization, thus reaching cut-off voltage in advance. In the absence of a CV process, cells with higher C-rate or lower ambient temperature have lower charging capacity. In addition, as can be seen from the local magnified image of Figure 5A, the increase of C-rate tends to lead to upward movement of the curve, making the reaction more intense; the decrease of ambient temperature tends to cause the curve to shift to the left, bringing forward the reaction. They all result in the cell reaching the cut-off voltage earlier. According to Equation 37, when the convective transfer coefficient h is 5 (W/m^{2}K) as natural convection, the temperature rise also increases with the increase of C-rate or the decrease of ambient temperature. For side reactions, as η_{lpl} decreases during charging, a danger zone, which indicated in blue in Figure 5C, is formed when η_{lpl} is below 0 V, with a risk of Li plating. Obviously, the C-rate is higher or

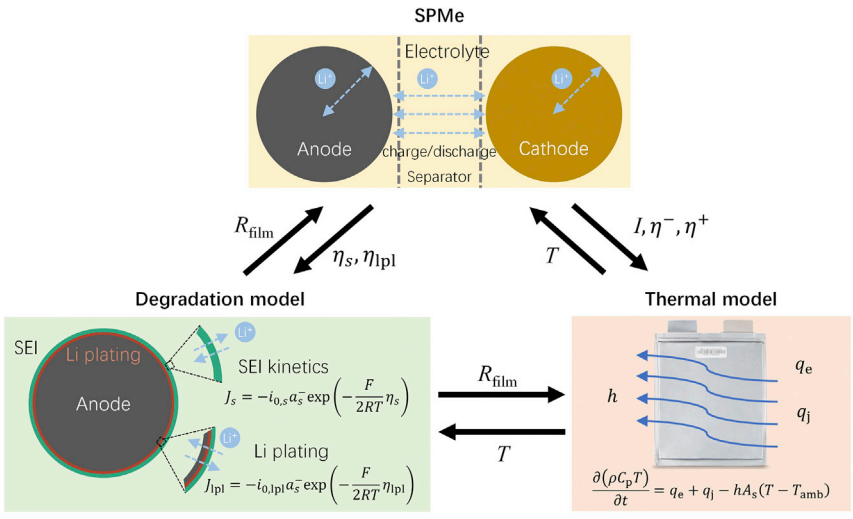

Figure 4. Coupling relationship of the three submodels of the single cell model

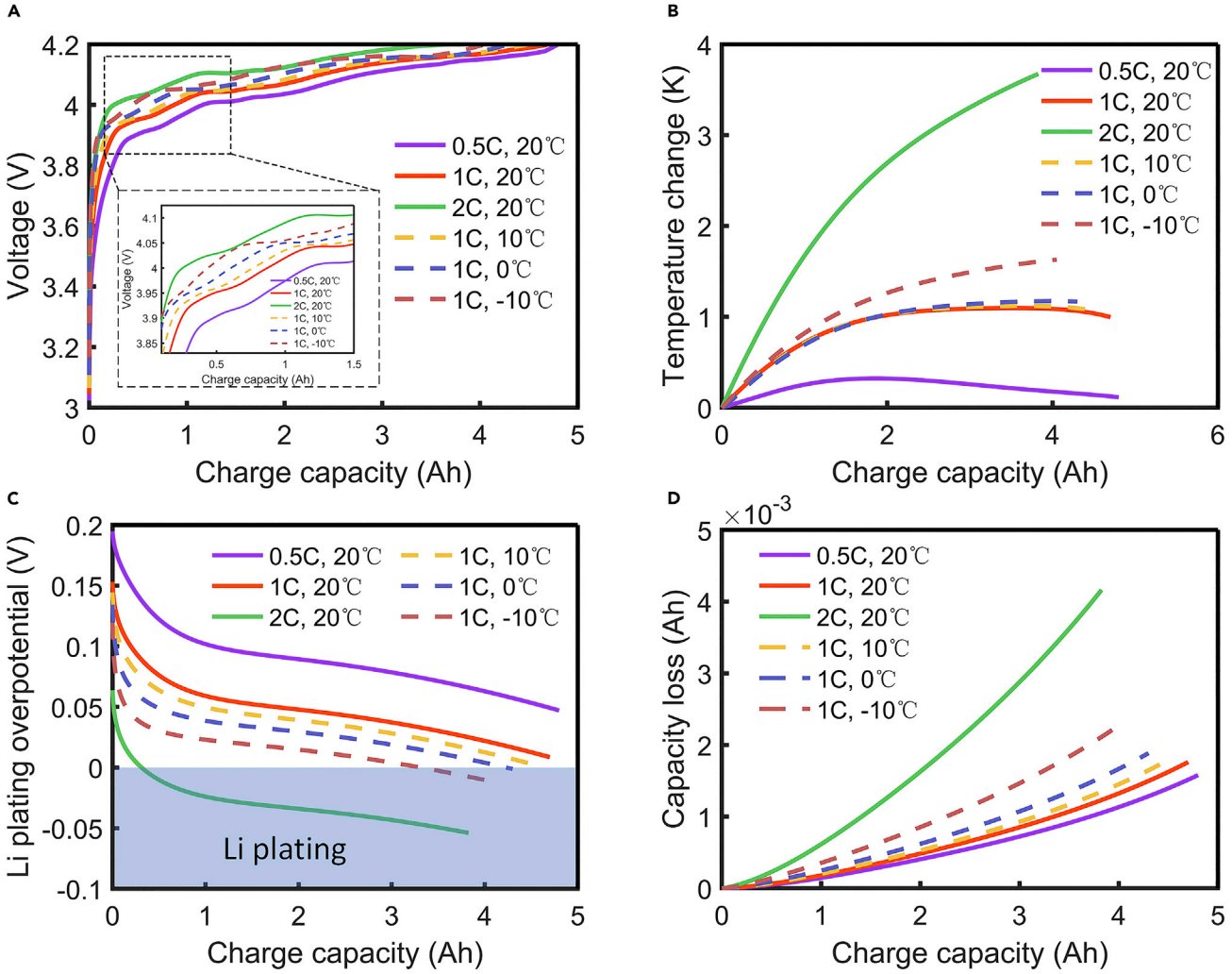

Figure 5. Simulation results of a single cell at different C-rates and different ambient temperatures

(A–D) (A)Voltage curve with charging capacity (V-Ah), (B) Temperature change, (C) Li plating overpotential, and (D) Capacity loss due to side reactions.

the ambient temperature is lower, and the risk of Li plating is greater. As shown in Figure 5C, under the charging condition of C-rate of 2C and ambient temperature of 20°C, the cell is at risk during most of the charging time, resulting in more severe capacity loss, as shown in Figure 5D. In contrast, under the ambient temperature of 20°C, η_{lpl} stays above 0 V all the time at the C-rate of 0.5C and 1C, whose capacity loss is mainly because of the growth of SEI film. At the same time, with the decrease of ambient temperature, Li plating overpotential will also be lower, increasing the risk of Li plating and the capacity loss. The aforementioned conclusions are in accordance with the law, the increase of C-rate or the decrease of ambient temperature will make the working conditions of the cell become bad, thus reducing the electrochemical performance (Wang et al., 2021b; Yu et al., 2022).

Parallel circuit model

The current distribution of parallel battery packs is complex and heterogeneous, mainly because of the differences between the cells in the battery pack and the specific circuit configurations. In this study, to discuss the battery pack control strategy, a circuit model of parallel battery pack is established, as shown in Figure 6. The battery pack model is composed of six cell models in parallel and each cell model is in a separate branch. Each branch uses a branch resistance R_b of 10 mΩ to describe the contact resistance between the connecting plate and the battery pole. The equations of the SPMe are integrated into the MATLAB environment, and the battery pack model is established in the Simulink SimPowerSystems toolbox. There is an

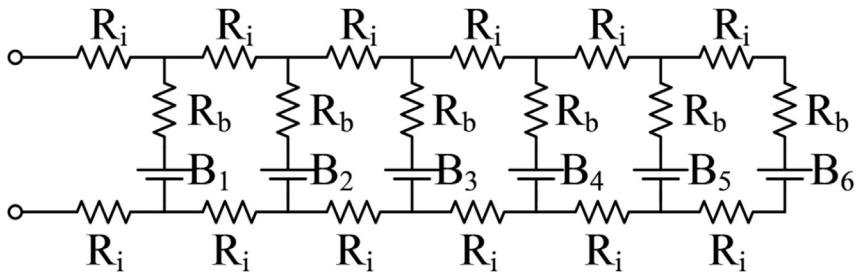

Figure 6. Circuit model diagram of parallel battery pack

interconnection resistance R_i of 0.5 mΩ indicating the influence of wire resistance at both ends of each branch. The current input and output are applied on the left side of the battery pack, with additional interconnection resistances at both ends. Voltage and current measuring tools are placed on each branch and the bus. It should be noted that the values of resistances were determined after referring to some literatures (Xie et al., 2021; Masomtob et al., 2017).

Here, the simulations of battery pack current distribution are carried out under different C-rates. The results under two C-rates (1C and 0.5C) are shown in Figure 7. The results for the other two C-rates (0.75C and 0.25C) are shown in Figure S1. The results show the serious heterogeneity of current distribution because of the particularity of parallel configuration. Similar trend of current distribution can be observed from curves of different C-rates. Cell B_1 usually has the largest fluctuation of current among the six cells. The current amplitudes of the six cells continued to show severe instability throughout the whole process. It should be noted that the branch currents fluctuated in Figure 7. This was because different branch currents at the beginning led to different charging or discharging capacities of each cell; that is, each cell had a different SOC. Considering the nonlinear OCV-SOC curve, the OCV variation of each cell was nonlinear and very complex. At the same time, there were also a series of inflection points and steps in the OCV curve (Li et al., 2021c). A series of factors caused the currents to fluctuate.

Charging strategy based on minimum Li plating overpotential control

Although charging technology has been greatly developed, most of the current research is applied to single cells, and there is little focus on the control strategy preventing side reactions during charging. When the overpotential of Li plating is close to 0 V or even lower, Li plating is easy to occur on the anode surface, resulting in irreversible capacity loss, and even short circuit inside the cell, threatening cell safety. The capacity loss caused by the growth of SEI film is more moderate than that caused by Li plating and occurs almost continuously throughout the cycle life. The growth of SEI film does not seriously affect battery safety. Therefore, based on the proposed electrochemical-side reactions-thermal coupling cell model, a parallel battery pack charging strategy based on minimum Li plating overpotential control (MLPOC) is adopted in this study to achieve the minimum Li plating control during rapid charging under various ambient temperatures, as shown in Figure 8, where I_{ini} is the initial input total current.

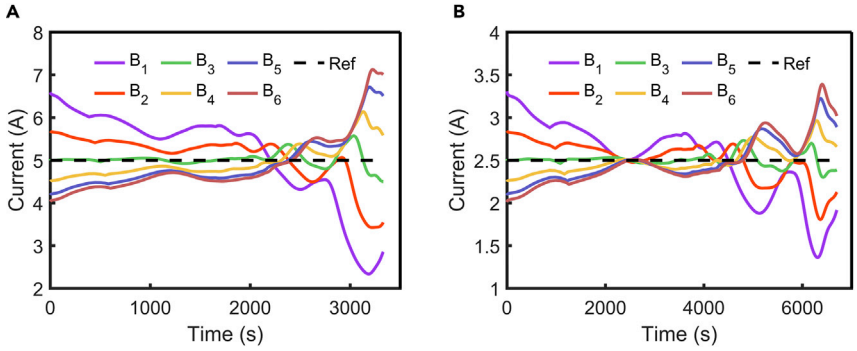

Figure 7. Simulation results of current distribution of a battery pack with six identical cells in parallel at different C-rates

(A and B) (A) 1 C and (B) 0.5 C.

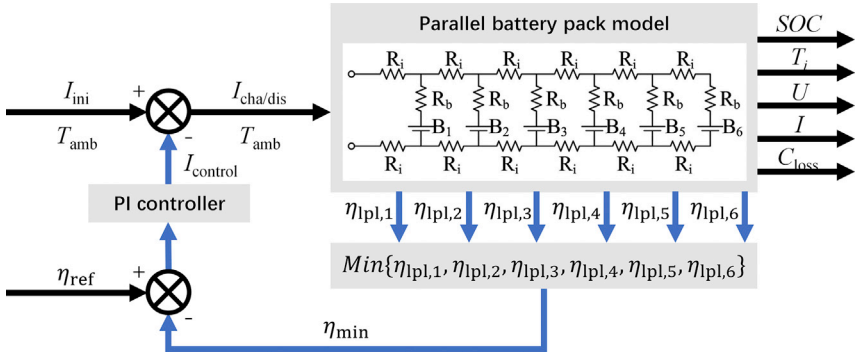

Figure 8. Charging strategy based on minimum Li plating overpotential control of a parallel battery pack

At the start of charging, a total current is input to the parallel battery pack model. Because the diffusion process has not been established at the start of charging, temperature only affects the electrochemical reaction. The temperature is lower, and the risk of Li plating is more. As the temperature rises, the overpotentials of reaction polarization and Li plating increase, resulting in the ability to withstand larger applied current without Li plating. However, the effect of electrochemical reaction on battery performance is limited, and when the ambient temperature varies within the conventional range, the proportional change in temperature in Kelvin is relatively small. Particle swarm optimization (PSO) algorithm was used to find the maximum initial charging current of a single cell under various ambient temperatures. According to the previous analysis, the maximum initial charging current changed monotonously with the increase of ambient temperature, so it was only necessary to find the current at the maximum and minimum temperatures. The temperature and initial conditions were set first, and then Li plating overpotential η_{lpl} was calculated according to the model. Finally, the maximum initial charging current was obtained when η_{lpl} equaled 0 V through iteration. When the ambient temperature range was −20°C–40°C, the maximum initial current of a single cell varied between 5.96 A–6.01 A, which is about 1.2C. Therefore, under different ambient temperatures, the initial charging current can be selected as the same value. For convenience, 2C was selected as the initial charging current in consideration of all charging situations such as directly charging after discharging without shelving. In other words, for a parallel battery pack, the initial input total current is the current of a cell multiplied by the number of branches. At the same time, as the charging process goes on, the overpotential will decrease, requiring subsequent control.

After the initial total current is input to the parallel battery pack, the Li plating overpotentials of all single cells are continuously monitored. The minimum value of all overpotentials is obtained through the minimum calculation module, which subtracts the reference value of Li plating 0 V. The result of subtraction is then entered into a proportional integration (PI) controller with a proportional parameter of 0.01 and an integral parameter of 0.00005. It should be noted that the parameters of the PI controller were obtained by the tuning method (Kull et al., 2020). Therefore, a closed loop optimization of charging current is realized by adjusting the charging current according to the output of the PI controller. It should be noted that in the charging process, the temperature will rise, which will affect the internal process of the cells. The PI controller can comprehensively control these effects. In addition, the external performance parameters of all cells are constantly logged into the workspace for further analysis.

DISCUSSION

Battery pack performance without MLPOC

To verify the control effect of MLPOC under various ambient temperatures, the simulations of battery pack with and without MLPOC under 2C and 1.5C was carried out under the ambient temperature of 0°C. Figure 9 shows the simulation results in one cycle under 2C and 0°C without MLPOC. When the average current is 1.5C, the simulation results without MLPOC in one cycle are shown in Figure S2. As shown in Figure 9A, the battery pack voltage is always below or above those of all the cells during the whole process, mainly because of the interconnection resistance between parallel branches. Figure 9B describes the change process of Li plating overpotentials. Combined with the changes of all the cells, in the late discharging process, the overpotentials presents a rising trend overall. This is because the cell temperatures increase with the working process, which improves the working environment of the cells to some extent. In addition, it

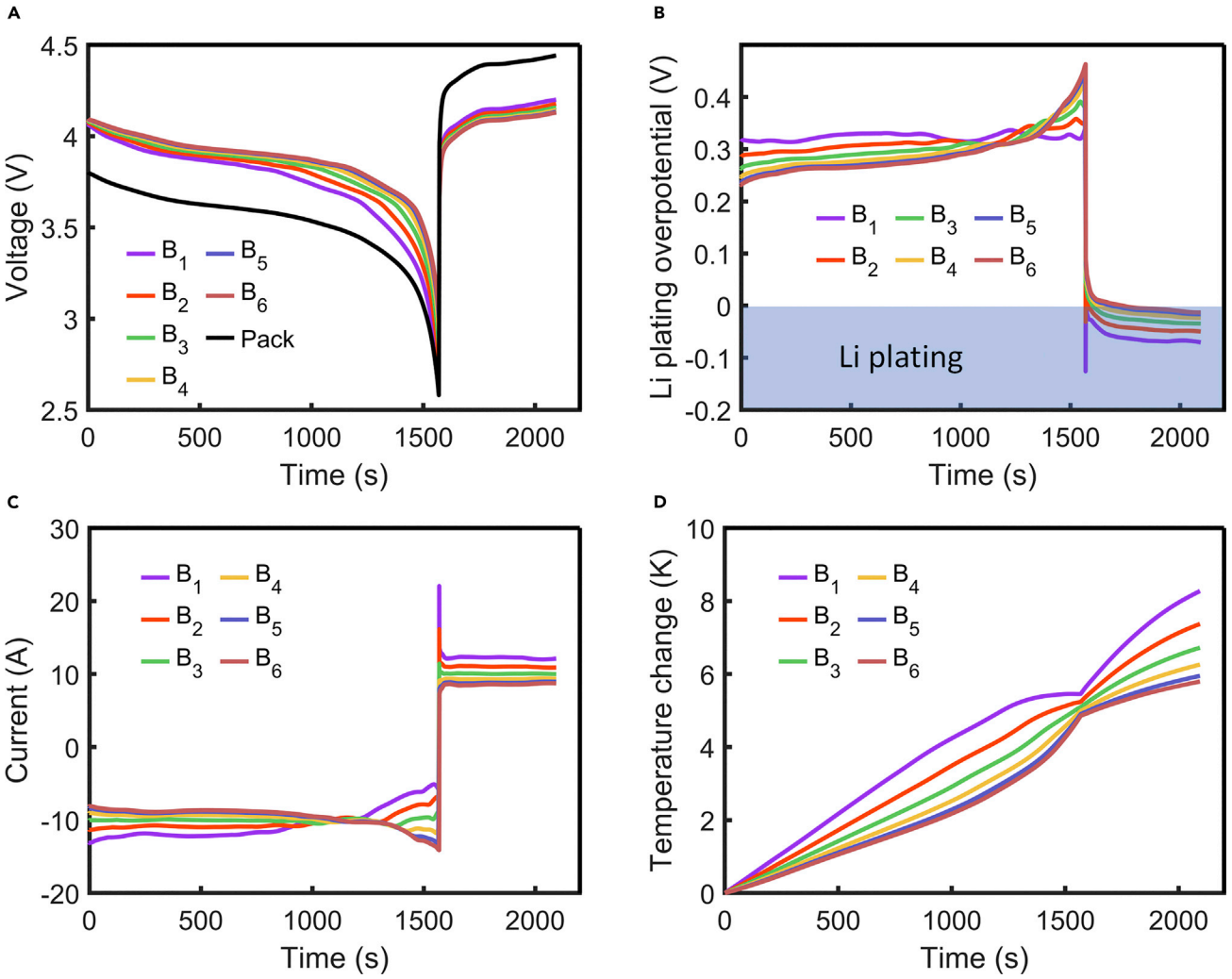

Figure 9. Simulation results without MLPOC under 2 C and 0°C

(A–D) (A) Voltage, (B) Li plating overpotential, (C) Current distribution, and (D) Temperature change.

can be seen that the Li plating overpotential of cell B_1 is below 0 V during the whole charging process, that is, it has the risk of Li plating during the whole charging process. As shown in Figure 9C, the current fluctuation of cell B_1 is the largest in the charging and discharging process. This is because the cell is located closest to the external structure in the parallel circuit and is most affected by the inconsistency of the battery pack. It should be noted that cell B_1 has the largest charging current of all cells at the start of charging, reaching 20 A (i.e., 4C). Figure 9D describes the temperature changes of the cells. Because the heat generation rate is closely related to the current, the temperature change is related to the current. For example, during the charging process, the current of cells B_1 and B_6 decreases and increases respectively, resulting in their heat generation rate decreases and increases respectively; and during discharging, the temperatures of the cells increase gradually. As shown in Figure S2D, the temperature of cell B_6 even decreases slightly at the end of discharging.

Obviously, with the higher current, the risk of Li plating is higher. In this case, Li plating overpotential of cell B_1 was negative during the charging process, and all cells would undergo Li plating to varying degrees, resulting in huge capacity loss. Without any control, side reactions can result in huge capacity loss and high safety risks under constant charging of high C-rate and low temperature. Specific quantitative analysis will be discussed in the next section. Therefore, for parallel battery packs, a reasonable active charging control strategy under various ambient temperatures is very necessary.

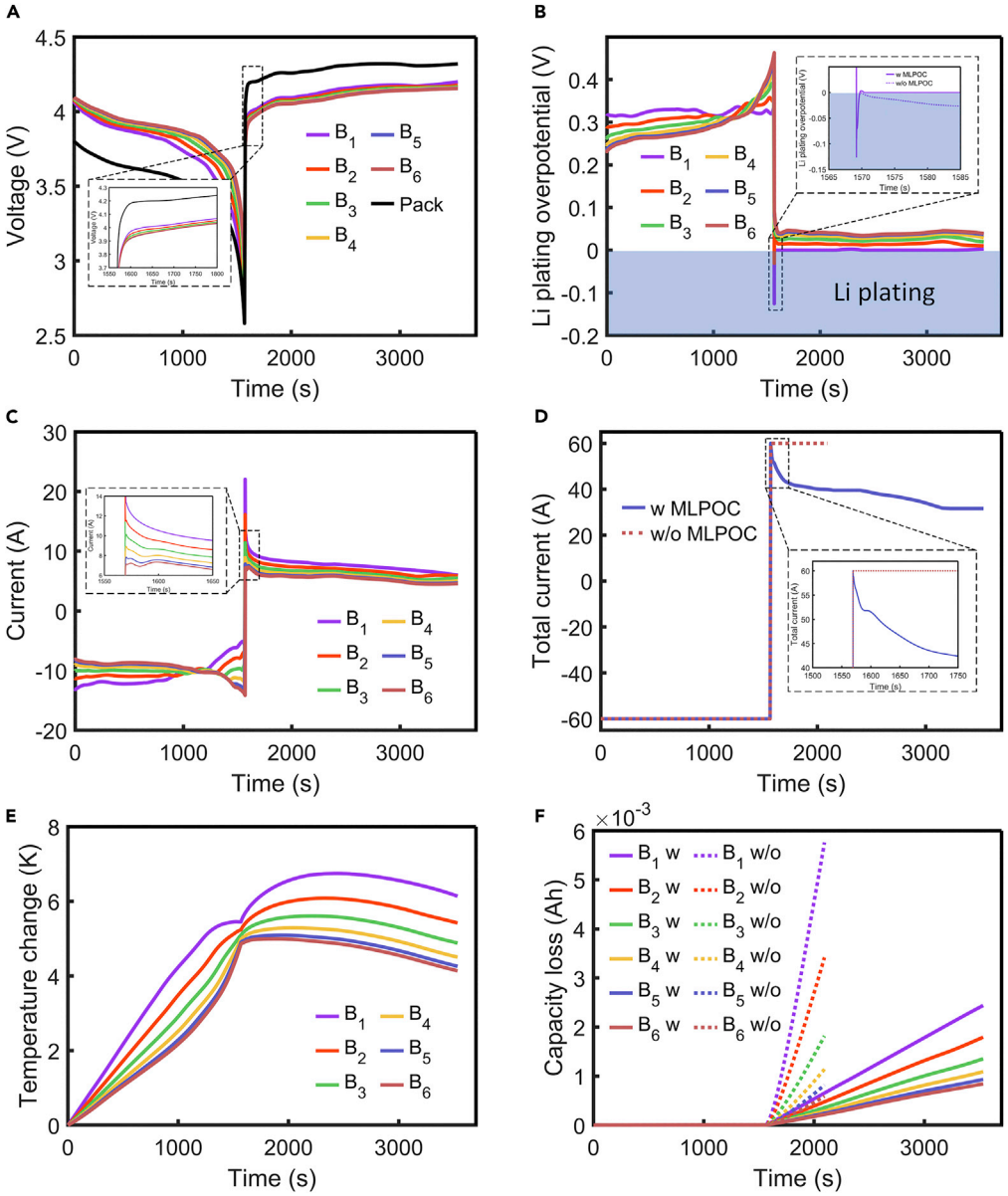

Figure 10. Simulation results with MLPOC and some without MLPOC under 2 C and 0°C

(A–F) (A) Voltage, (B) Li plating overpotential, (C) Current distribution, (D) Total current, (E) Temperature change, and (F) Capacity loss with and without MLPOC.

Battery pack performance with MLPOC

Figure 10 shows the simulation results of the battery pack model with MLPOC and some without MLPOC under 2C and 0°C in one cycle. At the beginning, the discharging process with MLPOC is identical with that of 2C without MLPOC. Once the charging process starts, the control strategy takes effect. As shown in Figure 10A, because of the use of MLPOC, the voltage does not rise rapidly at the start of charging as that without MLPOC. Figure 10B shows the change of Li plating overpotential during one cycle, especially comparing the Li plating overpotential of cell B_1 at the start of charging with and without MLPOC. In the local magnified image of Figure 10B, the solid line represents the Li plating overpotential with MLPOC, and the dotted line represents that without MLPOC. The sudden reversal of current may lead to a huge drop of Li plating overpotentials, in which the lowest overpotential immediately causes the response of the PI controller. This results in a corresponding interference signal, so that the input total current is reduced, which makes the minimum Li plating overpotential maintain at the reference value of 0 V. In

Table 1. Comparison of the charging process with or without MLPOC under 2C and 0°C

Charge scheme for parallel battery pack	Charge time (s)	Charge capacity (Ah)	Charge capacity rate (−)	Capacity loss (mAh)
2C and 0°C w/o MLPOC	525	9.41	31.37%	13.44
2C and 0°C w MLPOC	1964	20.50	68.33%	8.43

addition, the input total currents of the battery pack with and without MLPOC during the whole process are compared in Figure 10D. It should be noted that at the beginning of charging, the electrochemical reaction inside the cells was violent because there was no rest after discharging. It caused the Li plating overpotential curve in Figure 10B to drop sharply and then rise. Therefore, there would be a little Li plating at that time. However, it would not have a serious effect on the cells, because Li plating cannot be completely avoided (Chen et al., 2021) and can be restored (Hein et al., 2020). The variation of current distribution is shown in Figure 10C. Obviously, during charging, the current of cell B_1 is always the largest among all the branch currents, so cell B_1 becomes the cell with the lowest Li plating overpotential. Figure 10E shows the temperature change. As the charging current decreases, the heat generation rate decreases, and the cells are gradually difficult to maintain a high temperature. Thus, the temperatures of all the cells show a trend of decline in the late charging phase. If thermal management is added to the model to make the ambient temperature of the cells rise, the model can be further improved to increase the superiority of the control strategy. This is also the direction of further research. The capacity losses caused by side reactions with and without MLPOC are shown in Figure 10F. Without MLPOC, the branch currents of cells B_1 and B_2 are higher, resulting in a more severe capacity loss. At the same time, the inconsistency of current distribution leads to highly inconsistent degradation among the six cells. With MLPOC, the capacity loss and the inconsistency are significantly smaller. In addition, due to the maximum current, cell B_1 always has the greatest capacity loss.

As a comparison, the simulation results under 1.5C and 0°C are shown in Figure S3. It should be noted that 1.5C is close to the maximum initial charging current of a cell without Li plating, which is obtained in Chapter 3. Therefore, the capacity loss in the charging process under 1.5C is relatively mild compared with that under 2C. Nevertheless, MLPOC can eliminate the risk of Li plating successfully, which keeps the minimum Li plating overpotential at 0 V.

After the simulation, some indicators during the charging process are counted. The statistical results of 2C and 1.5C are shown in Tables 1 and S2, respectively. Table 1 shows the quantitative results of charging process indicators with and without MLPOC under 2C and 0°C. It should be noted that the CC-CV protocol was not used in this study, mainly because the CC-CV protocol would cause the current to drop when the voltage of cell B_1 reached the cut-off voltage of 4.2 V, which would lead to confusion and make it difficult to distinguish the contributions of MLPOC and the CV phase. Therefore, the results of MLPOC are only compared with those of the CC phase. Under 0°C and without MLPOC, the simulation results of charging capacity at CC stage show a downward trend with the increase of C-rate. However, lowering the charging current inevitably increases the cost of charging time, and there is no guarantee that Li plating will not occur. In contrast, MLPOC can increase charging capacity while ensuring minimal Li plating. For charging time, the charging capacity of the parallel battery pack is 20.50 Ah in 1964 s, which is equivalent to charging the battery pack at a constant current of 37.58 A (i.e., 1.25C). In addition, the effect is significantly better than the fast charging of CC-CV of 1C. In fact, compared with Tables 1 and S2, the final charging indicators of 2C and 1.5C are similar under 0°C with MLPOC, except that the capacity loss under 1.5C is a little better than that under 2C. This is because MLPOC controls the total current of charging. Comparing Figures 10D and S3D, the shape of the total current is very similar at the late charging phase. Therefore, the selected initial total current has little influence on MLPOC, whose influence is mainly reflected in the control results at the start of charging. If the initial total current of charging is selected too large, the minimum Li plating overpotential will be too small, resulting in very drastic current changes, which may cause damage to the hardware circuit. Therefore, it is important to choose the initial total current of charging reasonably.

Conclusions

This study established a battery model for a single cell by coupling a single particle model with electrolyte, degradation model, and thermal model, which could accurately describe battery performance under various ambient temperatures. On this basis, six cell models were connected in parallel, considering the

contact resistance and wire resistance, and the parallel battery model was established. A parallel battery pack charging strategy based on minimum potential was then adopted based on the provided model. It could achieve minimum Li plating overpotential control under various ambient temperatures to keep the minimum Li plating overpotential at 0 V. The ambient temperature and total current were input, and MLPOC took the minimum Li plating overpotential of all the cells as feedback for the controller, thus adjusting the input total current of the battery pack to avoid Li plating. Here, the PSO algorithm was used to find the maximum initial charging current of a cell under various ambient temperatures. Combined with the actual situation, an appropriate total current value for input was selected. Finally, the charging performances of battery packs with and without MLPOC were simulated at 1.5C and 2C under 0°C ambient temperature, and their results were compared. Comparative results showed that MLPOC could effectively keep the minimum Li plating overpotential at 0 V under various conditions, and reduced the capacity loss caused by Li plating. Although the charging time of MLPOC was relatively long, the total charging capacity of the parallel battery pack was improved. In addition, the charging time of MLPOC was still less than that of the CC-CV fast charging of 1C.

The charging strategy based on MLPOC fits with the battery digital twin framework. Sensors can be added to the batteries, which will realize the impact of physical entity to digital model to achieve digital twin. Meanwhile, it can also provide a new perspective for the application and promotion of V2G, which leaves room for further study.

Limitations of the study

This charging strategy was simulated only by a parallel circuit structure. Different circuit models may present different current distributions, which are worth studying in the future. At the same time, considering the interaction of the cells in the battery pack, the model of thermal management can be further added to the battery pack model to study the relationship between thermal management system and charging strategy in the future.

NOMENCLATURE

List of symbols

- a_s specific interfacial area (m^{-1})
- A_s convective surface area of the cell (m^2)
- c Li-ion concentration (mol m^{-3})
- C_p specific heat capacity (J kg^{-1} K^{-1})
- D diffusion coefficient (m^2 s^{-1})
- E_{act}^{Ψ} thermal activation energy corresponding to Ψ (J)
- F Faraday constant (C mol^{-1})
- h convective heat transfer coefficient (J m^{-2} s^{-1} K^{-1})
- I whole cell current externally provided (A)
- i whole cell current density externally provided (A m^{-2})
- i_{app} applied current density (A m^{-2})
- i_{lpl} reaction current density of Li plating (A m^{-2})
- i_s reaction current density of SEI growth (A m^{-2})
- $i_{0,lpl}$ exchange current density of Li plating (A m^{-2})
- $i_{0,s}$ exchange current density of SEI growth (A m^{-2})
- j_n molar ion flux (m^{-2} mol s^{-1})
- k reaction rate constant ($m^{2.5}$ $mol^{-0.5}$ s^{-1})
- L thickness of electrode (m)
- M_s molecular weight of SEI (kg mol^{-1})
- M_{lpl} molecular weight of Li metal (kg mol^{-1})
- r radius (m)
- R ideal gas constant (J mol^{-1} K^{-1})
- R_{film} SEI film resistance (Ω)
- $R_{film,0}$ initial SEI film resistance (Ω)
- R_s radius of electrode particle (m)
- t time (s)
- t_c^0 Li transference number (–)
- T cell temperature (K)
- T_{amb} ambient temperature (K)

T_{ref} reference temperature (K)
U equilibrium potential of electrode (V)
U_{lpl} equilibrium potential of Li plating (V)
U_s equilibrium potential of SEI growth (V)
V terminal voltage for single cell (V)
x stoichiometric number of electrode (–)

Greek letters

δ_{film} thickness of the film (m)
ε volume fraction (–)
η electrochemical overpotential (V)
η_{lpl} overpotential of Li plating (V)
η_s overpotential of SEI growth (V)
κ conductivity (S m^{-1})
κ_s conductivity of the film (S m^{-1})
ρ density of the cell (kg m^{-3})
ρ_{lpl} density of Li metal (kg m^{-3})
ρ_s density of SEI (kg m^{-3})
φ potential (V)
Ψ property of interest (unit that varies with the physical quantity)
Ψ_{ref} property value defined at the reference temperature T_{ref} (unit that varies with the physical quantity)

Superscripts

- anode, negative electrode
+ cathode, positive electrode
sep separator

Subscripts

s solid phase
e liquid phase
eff effective
sur surface
max maximum
n negative electrode
p positive electrode

STAR★METHODS

Detailed methods are provided in the online version of this paper and include the following:

- KEY RESOURCES TABLE
- RESOURCE AVAILABILITY
  - Lead contact
  - Materials availability
  - Data and code availability
- METHOD DETAILS
  - Single particle model with electrolyte
  - Degradation model
  - Thermal model

SUPPLEMENTAL INFORMATION

Supplemental information can be found online at https://doi.org/10.1016/j.isci.2022.104243.

ACKNOWLEDGMENTS

This work was financially supported by the Project funded by China Postdoctoral Science Foundation (2021M690740), the Weihai Scientific Research and Innovation Funds (2019KYCXJJYB09), and the National Natural Science Foundation of China (No. 52102470).

AUTHOR CONTRIBUTIONS

Conceptualization, H.Y. and X.L.; Writing – Original Draft, H.Y.; Revision, H.Y., L.Y., and J.L.; Validation, H.Y., L.Y., and L.Z.; Supervision, J.L. and X.L.; Funding Acquisition, J.L. and X.L.

DECLARATION OF INTERESTS

The authors declare no competing interests.

Received: January 26, 2022
Revised: March 21, 2022
Accepted: April 6, 2022
Published: May 20, 2022

REFERENCES

Bernardi, D., Pawlikowski, E., and Newman, J. (1985). A general energy balance for battery systems. J. Electrochem. Soc. *132*, 5. https://doi.org/10.1149/1.2113792. https://iopscience.iop.org/article/10.1149/1.2113792/meta.

Brand, M.J., Hofmann, M.H., Steinhardt, M., Schuster, S.F., and Jossen, A. (2016). Current distribution within parallel-connected battery cells. J. Power Sources *334*, 202–212. https://doi.org/10.1016/j.jpowsour.2016.10.010. https://www.sciencedirect.com/science/article/abs/pii/S0378775316313921.

Chen, W., Liang, J., Yang, Z., and Li, G. (2019). A review of lithium-ion battery for electric vehicle applications and beyond. Energy Proced. *158*, 4363–4368. https://doi.org/10.1016/j.egypro.2019.01.783. https://www.sciencedirect.com/science/article/pii/S1876610219308215.

Chen, S., Liu, T., Ge, J., Hong, J., and Wang, Y. (2021). Uniform distribution of Li deposition and high utilization of transferred metallic Li achieved by an unusual free-standing skeleton for high-performance Li metal batteries. ACS Appl. Energy Mater. https://doi.org/10.1021/acsaem.1c03041. https://pubs.acs.org/doi/abs/10.1021/acsaem.1c03041.

Chu, Z., Feng, X., Lu, L., Li, J., Han, X., and Ouyang, M. (2017). Non-destructive fast charging algorithm of lithium-ion batteries based on the control-oriented electrochemical model. Appl. Energy *204*, 1240–1250. https://doi.org/10.1016/j.apenergy.2017.03.111. https://www.sciencedirect.com/science/article/abs/pii/S0306261917303501.

Dang, X., Yan, L., Xu, K., Wu, X., Jiang, H., and Sun, H. (2016). Open-circuit voltage-based state of charge estimation of lithium-ion battery using dual neural network fusion battery model. Electrochim. Acta *188*, 356–366. https://doi.org/10.1016/j.electacta.2015.12.001. https://www.sciencedirect.com/science/article/abs/pii/S0013468615309257.

Dioha, M.O., Duan, L., Ruggles, T.H., Bellocchi, S., and Caldeira, K. (2022). Exploring the role of electric vehicles in Africa's energy transition: a Nigerian case study. iScience103926. https://doi.org/10.1016/j.isci.2022.103926. https://www.sciencedirect.com/science/article/pii/S2589004222001961.

Doyle, M., Fuller, T.F., and Newman, J. (1993). Modeling of galvanostatic charge and discharge of the lithium/polymer/insertion cell. J. Electrochem. Soc. *140*, 1526. https://doi.org/10.1149/1.2221597. https://iopscience.iop.org/article/10.1149/1.2221597/meta.

Dubarry, M., Devie, A., and Liaw, B.Y. (2016). Cell-balancing currents in parallel strings of a battery system. J. Power Sources *321*, 36–46. https://doi.org/10.1016/j.jpowsour.2016.04.125. https://www.sciencedirect.com/science/article/abs/pii/S0378775316305092.

Feng, X., Ren, D., He, X., and Ouyang, M. (2020). Mitigating thermal runaway of lithium-ion batteries. Joule *4*, 743–770. https://doi.org/10.1016/j.joule.2020.02.010. https://www.sciencedirect.com/science/article/pii/S254243512030088X.

Gao, X.L., Liu, X.H., Xie, W.L., Zhang, L.S., and Yang, S.C. (2021). Multiscale observation of Li plating for lithium-ion batteries. Rare Met. *40*, 3038–3048. https://doi.org/10.1007/s12598-021-01730-3. https://link.springer.com/article/10.1007/s12598-021-01730-3.

Ge, H., Aoki, T., Ikeda, N., Suga, S., Isobe, T., Li, Z., Tabuchi, Y., and Zhang, J. (2017). Investigating lithium plating in lithium-ion batteries at low temperatures using electrochemical model with NMR assisted parameterization. J. Electrochem. Soc. *164*, A1050. https://doi.org/10.1149/2.0461706jes. https://iopscience.iop.org/article/10.1149/2.0461706jes/meta.

Gottapu, M., Goh, T., Kaushik, A., Adiga, S.P., Bharathraj, S., Patil, R.S., Kim, D., and Ryu, Y. (2021). Fully coupled simplified electrochemical and thermal model for series-parallel configured battery pack. J. Energy Storage *36*, 102424. https://doi.org/10.1016/j.est.2021.102424. https://www.sciencedirect.com/science/article/abs/pii/S2352152X21001778.

Hein, S., Danner, T., and Latz, A. (2020). An electrochemical model of lithium plating and stripping in lithium ion batteries. ACS Appl. Energy Mater. *3*, 8519–8531. https://doi.org/10.1021/acsaem.0c01155. https://pubs.acs.org/doi/abs/10.1021/acsaem.0c01155.

Hosen, M.S., Jaguemont, J., Van Mierlo, J., and Berecibar, M. (2021). Battery lifetime prediction and performance assessment of different modeling approaches. iScience *24*, 102060. https://doi.org/10.1016/j.isci.2021.102060. https://www.sciencedirect.com/science/article/pii/S2589004221000286.

Hosseinzadeh, E., Arias, S., Krishna, M., Worwood, D., Barai, A., Widanalage, D., and Marco, J. (2021). Quantifying cell-to-cell variations of a parallel battery module for different pack configurations. Appl. Energy *282*, 115859. https://doi.org/10.1016/j.apenergy.2020.115859. https://www.sciencedirect.com/science/article/abs/pii/S0306261920313337.

Kull, T.M., Thalfeldt, M., and Kurnitski, J. (2020). PI parameter influence on underfloor heating energy consumption and setpoint tracking in nZEBs. Energies *13*, 2068. https://doi.org/10.3390/en13082068. https://www.mdpi.com/1996-1073/13/8/2068.

Li, Y., Feng, X., Ren, D., Ouyang, M., Lu, L., and Han, X. (2019). Thermal runaway triggered by plated lithium on the anode after fast charging. ACS Appl. Mater. Interfaces *11*, 46839–46850. https://doi.org/10.1021/acsami.9b16589. https://pubs.acs.org/doi/abs/10.1021/acsami.9b16589.

Li, L., Ren, Y., O'Regan, K., Koleti, U.R., Kendrick, E., Widanage, W.D., and Marco, J. (2021a). Lithium-ion battery cathode and anode potential observer based on reduced-order electrochemical single particle model. J. Energy Storage *44*, 103324. https://doi.org/10.1016/j.est.2021.103324. https://www.sciencedirect.com/science/article/pii/S2352152X21010161.

Li, Y., Li, K., Xie, Y., Liu, B., Liu, J., Zheng, J., and Li, W. (2021b). Optimization of charging strategy for lithium-ion battery packs based on complete battery pack model. J. Energy Storage *37*, 102466. https://doi.org/10.1016/j.est.2021.102466. https://www.sciencedirect.com/science/article/abs/pii/S2352152X21002164.

Li, J., Zhao, M., Dai, C., Wang, Z., and Pecht, M. (2021c). A mathematical method for open-circuit potential curve acquisition for lithium-ion batteries. J. Electroanal. Chem. *895*, 115488. https://doi.org/10.1016/j.jelechem.2021.115488. https://www.sciencedirect.com/science/article/abs/pii/S1572665721005142.

Liu, X., Ai, W., Marlow, M.N., Patel, Y., and Wu, B. (2019a). The effect of cell-to-cell variations and thermal gradients on the performance and degradation of lithium-ion battery packs. Appl. Energy *248*, 489–499. https://doi.org/10.1016/j.apenergy.2019.04.108. https://www.sciencedirect.com/science/article/abs/pii/S0306261919307810.

Liu, Y., Zhu, Y., and Cui, Y. (2019b). Challenges and opportunities towards fast-charging battery materials. Nat. Energy *4*, 540–550. https://doi.org/10.1038/s41560-019-0405-3. https://www.nature.com/articles/s41560-019-0405-3.

Lu, Q., Jie, Y., Meng, X., Omar, A., Mikhailova, D., Cao, R., Jiao, S., Lu, Y., and Xu, Y. (2021). Carbon materials for stable Li metal anodes: challenges, solutions, and outlook. Carbon Energy *3*, 957–975. https://doi.org/10.1002/cey2.147. https://onlinelibrary.wiley.com/doi/full/10.1002/cey2.147.

Masomtob, M., Sukondhasingha, R., Becker, J., and Sauer, D.U. (2017). Parametric study of spot welding between Li-ion battery cells and sheet metal connectors. Eng. J. *21*, 457–473. https://doi.org/10.4186/ej.2017.21.7.457. https://engj.org/index.php/ej/article/view/2053.

Nambisan, P., Saha, P., and Khanra, M. (2021). Real-time optimal fast charging of Li-ion batteries with varying temperature and charging behaviour constraints. J. Energy Storage *41*, 102918. https://doi.org/10.1016/j.est.2021.102918. https://www.sciencedirect.com/science/article/abs/pii/S2352152X21006320.

Nikdel, M. (2014). Various battery models for various simulation studies and applications. Renew. Sustain. Energy Rev. *32*, 477–485. https://doi.org/10.1016/j.rser.2014.01.048. https://www.sciencedirect.com/science/article/abs/pii/S1364032114000598.

Ouyang, Q., Wang, Z., Liu, K., Xu, G., and Li, Y. (2019). Optimal charging control for lithium-ion battery packs: a distributed average tracking approach. IEEE Trans. Ind. Inform. *16*, 3430–3438. https://doi.org/10.1109/TII.2019.2951060. https://ieeexplore.ieee.org/abstract/document/8889673/.

Peng, J.M., Chen, Z.Q., Li, Y., Hu, S.J., Pan, Q.C., Zheng, F.H., Wang, H.Q., and Li, Q.Y. (2021). Conducting network interface modulated rate performance in LiFePO4/C cathode materials. Rare Met. 1–9. https://doi.org/10.1007/s12598-021-01838-6. https://link.springer.com/article/10.1007/s12598-021-01838-6.

Reniers, J.M., Mulder, G., and Howey, D.A. (2019). Review and performance comparison of mechanical-chemical degradation models for lithium-ion batteries. J. Electrochem. Soc. *166*, A3189. https://doi.org/10.1149/2.0281914jes. https://iopscience.iop.org/article/10.1149/2.0281914jes/meta.

Schindler, M., Durdel, A., Sturm, J., Jocher, P., and Jossen, A. (2020). On the impact of internal cross-linking and connection properties on the current distribution in lithium-ion battery modules. J. Electrochem. Soc. *167*, 120542. https://doi.org/10.1149/1945-7111/abad6b. https://iopscience.iop.org/article/10.1149/1945-7111/abad6b/meta.

Shi, W., Hu, X., Jin, C., Jiang, J., Zhang, Y., and Yip, T. (2016). Effects of imbalanced currents on large-format LiFePO4/graphite batteries systems connected in parallel. J. Power Sources *313*, 198–204. https://doi.org/10.1016/j.jpowsour.2016.02.087. https://www.sciencedirect.com/science/article/abs/pii/S0378775316301951.

Tang, X., Wang, Y., Liu, Q., and Gao, F. (2021). Reconstruction of the incremental capacity trajectories from current-varying profiles for lithium-ion batteries. iScience *24*, 103103. https://doi.org/10.1016/j.isci.2021.103103. https://www.sciencedirect.com/science/article/pii/S2589004221010713.

Tomaszewska, A., Chu, Z., Feng, X., O'Kane, S., Liu, X., Chen, J., Ji, C., Endler, E., Li, R., Liu, L., et al. (2019). Lithium-ion battery fast charging: a review. eTransportation *1*, 100011. https://doi.org/10.1016/j.etran.2019.100011. https://www.sciencedirect.com/science/article/pii/S2590116819300116.

Wang, X., Wang, Z., Wang, L., Wang, Z., and Guo, H. (2019). Dependency analysis and degradation process-dependent modeling of lithium-ion battery packs. J. Power Sources *414*, 318–326. https://doi.org/10.1016/j.jpowsour.2019.01.021. https://www.sciencedirect.com/science/article/abs/pii/S0378775319300229.

Wang, J., Kang, Q., Yuan, J., Fu, Q., Chen, C., Zhai, Z., Liu, Y., Yan, W., Li, A., and Zhang, J. (2021a). Dendrite-free lithium and sodium metal anodes with deep plating/stripping properties for lithium and sodium batteries. Carbon Energy *3*, 153–166. https://doi.org/10.1002/cey2.94. https://onlinelibrary.wiley.com/doi/full/10.1002/cey2.94.

Wang, Y., Li, J., Zhang, J., and Pecht, M. (2021b). Lithium-iron-phosphate battery electrochemical modelling under a wide range of ambient temperatures. J. Electroanal. Chem. *882*, 115041. https://doi.org/10.1016/j.jelechem.2021.115041. https://www.sciencedirect.com/science/article/abs/pii/S1572665721000679.

Wu, B., Yufit, V., Marinescu, M., Offer, G.J., Martinez-Botas, R.F., and Brandon, N.P. (2013). Coupled thermal–electrochemical modelling of uneven heat generation in lithium-ion battery packs. J. Power Sources *243*, 544–554. https://doi.org/10.1016/j.jpowsour.2013.05.164. https://www.sciencedirect.com/science/article/abs/pii/S0378775313009622.

Wu, B., Widanage, W.D., Yang, S., and Liu, X. (2020). Battery digital twins: perspectives on the fusion of models, data and artificial intelligence for smart battery management systems. Energy AI *1*, 100016. https://doi.org/10.1016/j.egyai.2020.100016. https://www.sciencedirect.com/science/article/pii/S2666546820300161.

Wu, X., Cui, Z., Zhou, G., Wen, T., Hu, F., Du, J., and Ouyang, M. (2021). Comprehensive early warning strategies based on consistency deviation of thermal–electrical characteristics for energy storage grid. iScience *24*, 103058. https://doi.org/10.1016/j.isci.2021.103058. https://www.sciencedirect.com/science/article/pii/S2589004221010269.

Xie, W., Liu, X., He, R., Li, Y., Gao, X., Li, X., Peng, Z., Feng, S., Feng, X., and Yang, S. (2020). Challenges and opportunities toward fast-charging of lithium-ion batteries. J. Energy Storage *32*, 101837. https://doi.org/10.1016/j.est.2020.101837. https://www.sciencedirect.com/science/article/abs/pii/S2352152X20316741.

Xie, Y., Wang, X., Hu, X., Li, W., Zhang, Y., and Lin, X. (2021). An enhanced electro-thermal model for EV battery packs considering current distribution in parallel branches. IEEE Trans. Power Electron. *37*, 1027–1043. https://doi.org/10.1109/TPEL.2021.3102292. https://ieeexplore.ieee.org/abstract/document/9508844.

Yan, X., Lin, L., Chen, Q., Xie, Q., Qu, B., Wang, L., and Peng, D.L. (2021). Multifunctional roles of carbon-based hosts for Li-metal anodes: a review. Carbon Energy *3*, 303–329. https://doi.org/10.1002/cey2.95. https://onlinelibrary.wiley.com/doi/full/10.1002/cey2.95.

Yang, X.G., Liu, T., Gao, Y., Ge, S., Leng, Y., Wang, D., and Wang, C.Y. (2019). Asymmetric temperature modulation for extreme fast charging of lithium-ion batteries. Joule *3*, 3002–3019. https://doi.org/10.1016/j.joule.2019.09.021. https://www.sciencedirect.com/science/article/pii/S2542435119304817.

Yang, S., He, R., Zhang, Z., Cao, Y., Gao, X., and Liu, X. (2020). CHAIN: cyber hierarchy and interactional network enabling digital solution for battery full-lifespan management. Matter *3*, 27–41. https://doi.org/10.1016/j.matt.2020.04.015. https://www.sciencedirect.com/science/article/pii/S2590238520301867.

Yang, S., Gao, X., Li, Y., Xie, W., Guo, B., Zhang, L., and Liu, X. (2021). Minimum lithium plating overpotential control based charging strategy for parallel battery module prevents side reactions. J. Power Sources *494*, 229772. https://doi.org/10.1016/j.jpowsour.2021.229772. https://www.sciencedirect.com/science/article/abs/pii/S037877532100313X.

Yu, H., Li, J., Ji, Y., and Pecht, M. (2022). Life-cycle parameter identification method of an electrochemical model for lithium-ion battery pack. J. Energy Storage *47*, 103591. https://doi.org/10.1016/j.est.2021.103591. https://www.sciencedirect.com/science/article/abs/pii/S2352152X2101269X.

Zhang, D., Popov, B.N., and White, R.E. (2000). Modeling lithium intercalation of a single spinel particle under potentiodynamic control. J. Electrochem. Soc. *147*, 831. https://doi.org/10.1149/1.1393279. https://iopscience.iop.org/article/10.1149/1.1393279/meta.

Zhang, C., Jiang, J., Gao, Y., Zhang, W., Liu, Q., and Hu, X. (2017). Charging optimization in lithium-ion batteries based on temperature rise and charge time. Appl. Energy *194*, 569–577. https://doi.org/10.1016/j.apenergy.2016.10.059. https://www.sciencedirect.com/science/article/abs/pii/S0306261916315033.

Zhao, Y., Zhang, Y., Wang, Y., Cao, D., Sun, X., and Zhu, H. (2021). Versatile zero-to three-dimensional carbon for electrochemical energy storage. Carbon Energy *3*, 895–915. https://doi.org/10.1002/cey2.137. https://onlinelibrary.wiley.com/doi/full/10.1002/cey2.137.

Zhou, C.C., Su, Z., Gao, X.L., Cao, R., Yang, S.C., and Liu, X.H. (2022). Ultra-high-energy lithium-ion batteries enabled by aligned structured thick electrode design. Rare Met. *41*, 14–20. https://doi.org/10.1007/s12598-021-01785-2. https://link.springer.com/article/10.1007/s12598-021-01785-2.

STAR★METHODS

KEY RESOURCES TABLE

REAGENT or RESOURCE	SOURCE	IDENTIFIER
Software and algorithms		
MATLAB 2019b	MathWorks	https://www.mathworks.com/products/matlab.html
PID Controller	MathWorks	https://www.mathworks.com/help/simulink/slref/pidcontroller.html

RESOURCE AVAILABILITY

Lead contact

Further information and requests for resources and reagents should be directed to and will be fulfilled by the lead contact, Xinhua Liu (liuxinhua19@buaa.edu.cn).

Materials availability

This study did not generate new materials.

Data and code availability

No additional data was used. This paper does not report original code. Any additional information for re-analyzing this work is available from the lead contact upon request.

METHOD DETAILS

The single cell model consists of SPMe, degradation model and thermal model, explained in detail in this section. It should be noted that the processes in the following equations are related to time, and the time variable t is not written in the processes for convenience.

Single particle model with electrolyte

The terminal voltage of the battery is calculated by the solid phase potentials φ_s, as shown in (Equation 1). According to the electrochemical overpotentials η and equilibrium potentials U, the solid phase potentials of cathode and anode are defined as Equations (2) and (3), which are related to the state of lithiation. Note that due to considering side reactions, the total current density i is the sum of the applied current density i_{app}, SEI growth current density i_s, and Li plating current density i_{lpl}, as shown in (Equation 4). At the same time, it should be noted that the resistance of the film on the cathode is ignored due to the little effect.

$$V = \varphi_s^+ - \varphi_s^- \quad \text{(Equation 1)}$$

$$\varphi_s^+ = \eta^+ + \varphi_e^+ + U^+ \quad \text{(Equation 2)}$$

$$\varphi_s^- = \eta^- + \varphi_e^- + U^- + \frac{R_{film} i}{a_s^- L^-} \quad \text{(Equation 3)}$$

$$i = i_{app} + i_s + i_{lpl} \quad \text{(Equation 4)}$$

The electrochemical overpotentials for anode and cathode follow the Butler-Volmer (BV) equation, which can be approximated as Equations (5) and (6). The equilibrium potentials are related to the state of lithiation of the electrodes. The equilibrium potential of the anode adopts a fitting function, as shown in (Equation 7). The stoichiometry of the anode x_n is defined by the surface and maximum lithium concentration of the solid phase, as shown in (Equation 8). The equilibrium potential and x_p of the cathode were tested by the half-cell experiment, which can be found in our previous study (Liu et al., 2019a).

$$\eta^- = \frac{2RT}{F}\sinh^{-1}\left(\frac{j_n^-}{2k_{eff}^-\sqrt{c_e c_{s,sur}^-\left(c_{s,max}^- - c_{s,sur}^-\right)}}\right) \quad \text{(Equation 5)}$$

$$\eta^{+} = \frac{2RT}{F}\sinh^{-1}\left(\frac{j_n^{+}}{2k_{eff}^{+}\sqrt{c_e c_{s,sur}^{+}\left(c_{s,\max}^{+} - c_{s,sur}^{+}\right)}}\right) \quad \text{(Equation 6)}$$

$$U^{-} = 0.7222 + 0.1387x_n + 0.029x_n^{0.5} - \frac{0.0172}{x_n} + \frac{0.0019}{x_n^{1.5}} + 0.2808e^{(0.9-15x_n)} - 0.7984e^{(0.4465x_n-0.4108)} \quad \text{(Equation 7)}$$

$$x_n = \frac{c_{s,sur}^{-}}{c_{s,\max}^{-}} \quad \text{(Equation 8)}$$

As mentioned above, the active material for each electrode is assumed to be a particle. The diffusion in the solid phase follows the Fick's law as (Equation 9), and the boundary conditions for both anode and cathode can be expressed as Equations (10) and (11). At the particle surface, the flux of lithium-ion concentration is related to the applied current; while at the particle center, the flux of lithium-ion concentration is not allowed.

$$\frac{\partial c_s^{\pm}}{\partial t} = \frac{1}{r^2}\frac{\partial}{\partial r}\left[D_s^{\pm} r^2 \frac{\partial c_s^{\pm}}{\partial r}\right] \quad \text{(Equation 9)}$$

$$\frac{\partial c_s^{\pm}}{\partial r} = 0, (r = 0) \quad \text{(Equation 10)}$$

$$\frac{\partial c_s^{\pm}}{\partial r} = \pm\frac{i_{\text{app}}}{D_s^{\pm} F a_s^{\pm} L^{\pm}}, \left(r = R_s^{\pm}\right) \quad \text{(Equation 11)}$$

The diffusion of lithium-ion in the liquid phase follows (Equation 12). The boundary conditions of the entire battery domain can be expressed as Equations 13, 14, 15, 16, and 17. It should be noted that c_e represents the lithium-ion concentration in the liquid phase, and the superscript of c_e represents different regions of the battery. The boundary conditions are as follows: (1) at the boundary positions where the two electrode regions contact with the current collectors, there are no liquid lithium-ion concentration gradients in the x direction; (2) at the junctions of the anode and the separator as well as the cathode and the separator, the liquid lithium-ion concentrations on both sides of the interfaces are equal, and the concentration gradients are also equal considering the property of the pore.

$$\varepsilon_e^j \frac{\partial c_e}{\partial t} = \frac{\partial}{\partial x}\left[D_{e,eff}^j \frac{\partial c_e}{\partial x} + \frac{1 - t_c^0}{F} i_e^j\right], j \in \{-, sep, +\} \quad \text{(Equation 12)}$$

$$\frac{\partial c_e(0)}{\partial x} = \frac{\partial c_e(L^- + L^{sep} + L^+)}{\partial x} = 0 \quad \text{(Equation 13)}$$

$$c_e^{-}(L^-) = c_e^{sep}(L^-) \quad \text{(Equation 14)}$$

$$c_e^{sep}(L^- + L^{sep}) = c_e^{+}(L^- + L^{sep}) \quad \text{(Equation 15)}$$

$$D_{e,eff}^{-}\frac{\partial c_e^{-}(L^-)}{\partial x} = D_{e,eff}^{sep}\frac{\partial c_e^{sep}(L^-)}{\partial x} \quad \text{(Equation 16)}$$

$$D_{e,eff}^{sep}\frac{\partial c_e^{sep}(L^- + L^{sep})}{\partial x} = D_{e,eff}^{+}\frac{\partial c_e^{+}(L^- + L^{sep})}{\partial x} \quad \text{(Equation 17)}$$

Where, t_c^0 is the Li transference number, $D_{e,eff}^j = D_e \cdot (\varepsilon_e^j)^{1.5}$ is the effective liquid phase diffusion coefficient of lithium-ion, which is given by Bruggeman relation. The ionic current densities i_e in the regions for anode and cathode are shown in (Equation 18), and its boundary conditions are shown in (Equation 19), where j_n is molar ion flux. There is no molar ion flux in the diaphragm region, i.e., $\frac{\partial i_e^{sep}}{\partial x} = 0$.

$$\frac{\partial i_e^{\pm}}{\partial x} = a_s^{\pm} F j_n^{\pm} \quad \text{(Equation 18)}$$

$$i_e^{-}(0) = i_e^{+}(L^- + L^{sep} + L^+) = 0 \quad \text{(Equation 19)}$$

Based on the above Assumption [A2], it can be further concluded that $j_n^{\pm}$ is a fixed value in the corresponding electrode region and does not change with the position in the direction of the electrode plate thickness. By combining Equations (18) and (19), it can be expressed that the molar ion flux is proportional to the current, as shown in (Equation 20). Therefore, the distribution of ion current density i_e and molar ion flux j_n in the direction of the electrode plate thickness are shown in Figure 2.

$$j_n^{+} = -\frac{i_{\text{app}}}{F a_s^{+} L^{+}}, j_n^{-} = \frac{i_{\text{app}}}{F a_s^{-} L^{-}} \quad \text{(Equation 20)}$$

By combining Equations (12), (18) and (20), the liquid phase diffusion equation of lithium-ion can be deduced as shown in Equations 21, 22, and 23, and the boundary conditions are the same as Equations 13, 14, 15, 16, and 17. Here, the SPMe model contains partial differential equations (PDEs) to represent the concentration, which can be solved by finite difference method or finite volume method.

$$\frac{\partial c_e^{-}}{\partial t} = \frac{\partial}{\partial x}\left[\frac{D_{e,eff}^{-}}{\varepsilon_e^{-}}\frac{\partial c_e^{-}}{\partial x}\right] + \frac{1 - t_c^0}{\varepsilon_e^{-} FL^{-}} i_{app} \quad \text{(Equation 21)}$$

$$\frac{\partial c_e^{sep}}{\partial t} = \frac{\partial}{\partial x}\left[\frac{D_{e,eff}^{sep}}{\varepsilon_e^{sep}}\frac{\partial c_e^{sep}}{\partial x}\right] \quad \text{(Equation 22)}$$

$$\frac{\partial c_e^{+}}{\partial t} = \frac{\partial}{\partial x}\left[\frac{D_{e,eff}^{+}}{\varepsilon_e^{+}}\frac{\partial c_e^{+}}{\partial x}\right] - \frac{1 - t_c^0}{\varepsilon_e^{+} FL^{+}} i_{app} \quad \text{(Equation 23)}$$

The PDE of the electrolyte potential is shown in (Equation 24), whose boundary conditions are shown in Equations 25, 26, and 27. The PDE describes the process of the liquid phase lithium-ion conduction in the regions of the anode, separator, and cathode.

$$\kappa_{eff}^{j}\frac{\partial \varphi_e}{\partial x} = -i_e^{j} + \kappa_{eff}^{j}\frac{2RT}{F}\left(1 - t_c^0\right)\frac{\partial \ln c_e}{\partial x}, j \in \{-, sep, +\} \quad \text{(Equation 24)}$$

$$\varphi_e^{-}(0) = 0 \quad \text{(Equation 25)}$$

$$\varphi_e^{-}(L^{-}) = \varphi_e^{sep}(L^{-}) \quad \text{(Equation 26)}$$

$$\varphi_e^{sep}(L^{-} + L^{sep}) = \varphi_e^{+}(L^{-} + L^{sep}) \quad \text{(Equation 27)}$$

Where, $\kappa_{eff}^{j} = \kappa \cdot (\varepsilon_e^{j})^{1.5}$ is the effective liquid phase conductivity of lithium-ion, which is given by Bruggeman relation. The electrolyte potential difference is obtained by integrating (Equation 24) with respect to x across the entire cell width:

$$\varphi_e^{+} - \varphi_e^{-} = -\left(\frac{L^{-}}{2\kappa_{eff}^{-}} + \frac{L^{sep}}{\kappa_{eff}^{sep}} + \frac{L^{+}}{2\kappa_{eff}^{+}}\right) i_{app} + \frac{2RT}{F}\left(1 - t_c^0\right)\ln\frac{c_e(L^{-} + L^{sep} + L^{+})}{c_e(0)} \quad \text{(Equation 28)}$$

The liquid phase potential difference can be calculated by substituting the calculated liquid phase lithium-ion concentration. At this point, the required calculated physical quantities are substituted into (Equation 1) to find the corresponding terminal voltage value. It should be noted that the output of terminal voltage is only a nonlinear function of current, and other variables are parameters or current dependent.

A block diagram of SPMe is shown in Figure 3. The model includes: (1) two spherical diffusion PDEs which simulate the electrode dynamics of solid phase concentration distribution; (2) PDEs across three regions which simulate the electrolyte dynamics of liquid phase concentration distribution; (3) a nonlinear output function which maps conditions, such as solid phase concentration, liquid phase concentration, and current boundary value, to voltage. It should be noted that the c_s^{+}, c_s^{-}, c_e subsystems in Figure 3 are independent of each other.

Degradation model

In this model, we assume that the main degradation modes can be attributed to the growth of SEI film and Li plating on the anode surface, which consume recyclable lithium by thickening the passivation layer and forming Li dendrites, respectively. These two side reactions can cause permanent capacity loss externally, or even lead to catastrophic accidents like thermal runaway under some extreme conditions such as fast charging and low temperature charging (Li et al., 2019).

In general, the growth of SEI film and the reaction of Li plating can be described by BV equation with Tafel approximation, as shown in Equations (29) and (31) respectively, where their overpotential can be defined as Equations (30) and (32) respectively. To be clear, $i_{0,s}$ and $i_{0,lpl}$ represent the current density of the reactions. Note that the equilibrium potentials of SEI film and Li metal are assumed to be 0.4 V and 0 V, respectively (Yang et al., 2021). When the driving overpotential of Li plating becomes negative, the Li plating reaction will be triggered (Ge et al., 2017).

$$J_s = -i_{0,s} a_s^{-} \exp\left(-\frac{F}{2RT}\eta_s\right) \quad \text{(Equation 29)}$$

$$\eta_s = \varphi_s^{-} - \varphi_e^{-} - U_s - \frac{J}{a_s^{-}} R_{film} \quad \text{(Equation 30)}$$

$$J_{lpl} = -i_{0,lpl} a_s^- \exp\left(-\frac{F}{2RT}\eta_{lpl}\right) \quad \text{(Equation 31)}$$

$$\eta_{lpl} = \varphi_s^- - \varphi_e^- - U_{lpl} - \frac{J}{a_s^-} R_{film} \quad \text{(Equation 32)}$$

The film thickness growth rate and the resistance can be described as a combination of the two side reactions, as shown in Equations (33) and (34). To be clear, M_s and M_{lpl} are the molecular weights of SEI film and Li metal respectively; ρ_s and ρ_{lpl} are the densities of the two substances respectively; κ_s is the conductivity of the film.

$$\frac{\partial \delta_{film}}{\partial t} = -\frac{J_s M_s}{a_s^- \rho_s F} - \frac{J_{lpl} M_{lpl}}{a_s^- \rho_{lpl} F} \quad \text{(Equation 33)}$$

$$R_{film} = R_{film,0} + \frac{\delta_{film}}{\kappa_s} \quad \text{(Equation 34)}$$

Thermal model

The heat generated by LIBs in the working process can be divided into two categories: reversible heat and irreversible heat (Reniers et al., 2019). Reversible heat is due to the entropy change of open circuit voltage with temperature change. Irreversible heat is generated by the overpotentials, which includes ohmic heat, enthalpy heat, reaction heat and mixing heat. For convenience, the thermal model is simplified in this paper. Considering the stable electrochemical performance, good transmission characteristics and limited concentration gradient of commercial batteries, the heat generated by entropy change, enthalpy heat and mixing heat can be ignored. The ohmic heat and reaction heat considered are defined as Equations (35) and (36), and the energy balance law is described as (Equation 37), where C_p is specific heat capacity, h is convective heat transfer coefficient, A_s is convective surface area, T is battery Temperature, and T_{amb} is ambient temperature. It should be noticed that the interaction of temperature among cells is not considered in this battery pack model. That is because the temperature change of the simulated cell is small, and the battery pack has fewer cells and simple structure which is the cells in a row.

$$q_e = I^2 R_{film} \quad \text{(Equation 35)}$$

$$q_j = I(\eta^- - \eta^+) \quad \text{(Equation 36)}$$

$$\frac{\partial(\rho C_p T)}{\partial t} = q_e + q_j - hA_s(T - T_{amb}) \quad \text{(Equation 37)}$$

The effect of temperature on the electrochemical process can be described by Arrhenius equation, as shown in (Equation 38), where the Ψ_{ref} represents the property of a parameter at the reference temperature.

$$\Psi = \Psi_{ref} \exp\left[\frac{E_{act}^{\Psi}}{R}\left(\frac{1}{T_{ref}} - \frac{1}{T}\right)\right] \quad \text{(Equation 38)}$$